"Characterization of AlSi10Mg interlocking structures additively manufactured via Laser Powder Bed Fusion"

Available online at www.sciencedirect.com

ScienceDirect

Procedia CIRP 00 (2024) 000–000

www.elsevier.com/locate/procedia

18th CIRP Conference on Intelligent Computation in Manufacturing Engineering

Characterization of AlSi10Mg interlocking structures additively manufactured via Laser Powder Bed Fusion

Federica Valenza[a,b,c,*], Alberta Aversa[b,c], Eleonora Atzeni[a,c], Sara Biamino[b,c], Gabriele Piscopo[a,c], Alessandro Salmi[a,c]

[a]*Politecnico di Torino, Department of Management and Production Engineering (DIGEP), Corso Duca degli Abruzzi 24, 10129 Torino, Italy*
[b]*Politecnico di Torino, Department of Applied Science and Technology (DISAT), Corso Duca degli Abruzzi 24, 10129 Torino, Italy*
[c]*Politecnico di Torino, Interdepartmental Center for Integrated Additive Manufacturing (IAM@Polito), Corso Castelfidardo 51, 10129 Torino, Italy*

* Corresponding author. Tel.: +39 011 090.7280; fax: +39 011 090.7299. *E-mail address:* federica.valenza@polito.it

Abstract

Mechanical interlocking is a joining technique capable of mechanically bonding two dissimilar materials by means of protrusions on the component surfaces, as an alternative or complement to mechanical fasteners or adhesives. Proper adhesion between materials, and joint retention mainly depend on the shape and strength of the interlocking structures. In this respect, additive manufacturing is used to optimize the interlocking design and performance. The intent of this research is to evaluate the effectiveness of laser powder bed fusion and post-processing treatments on AlSi10Mg interlocking structures. The geometry, microstructure and density of the structures are investigated utilizing metallographic and tomographic techniques.

Peer-review under responsibility of the scientific committee of the 18th CIRP Conference on Intelligent Computation in Manufacturing Engineering, 10-12 July, Gulf of Naples, Italy

Keywords: Additive Manufacturing; Laser Powder Bed Fusion; Mechanical Interlocking; AlSi10Mg.

1. Introduction

In recent years, there has been an increasing demand for lightweight and high-performance components in various industrial domains, to meet climate targets and adhere to the principles of the green economy [1]. A promising approach involves joining dissimilar materials, such as polymers to metals, in order to create tailor-made functional components. These hybrid structures are gaining interest in automotive and aerospace applications, reflecting the shift towards sustainability and efficiency in reducing fuel consumption and CO_2 emissions [2]. Bonding dissimilar materials, however, can be challenging due to inherent differences in physical properties and compositions. While mechanical fastening and adhesive bonding are commonly used for material joining, each of these methods has specific limitations. Mechanical fastening, for example, introduces issues such as the stress concentration at fastening points, the material damage caused by machining operations, and the added weight from rivets and bolts. Adhesive bonding, conversely, requires surface preparation and may necessitate costly quality control procedures. Additionally, adhesives can degrade over time, particularly in hot and wet environments. As a result, there is interest in developing alternative joining solutions that can overcome these limitations [3].

An innovative technology currently being explored as a potential alternative to conventional joining methods and here investigated is mechanical interlocking. This approach relies on physically interlocking components by properly designed arrays of macro-scale features protruding from the surface of the materials to be joined. An important advantage of this technique is its proven ability to strengthen the interfacial bond

Peer-review under responsibility of the scientific committee of the 18th CIRP Conference on Intelligent Computation in Manufacturing Engineering, 10-12 July, Gulf of Naples, Italy

between different materials, thereby eliminating the need for additional locking elements [4]. Various techniques can be employed to produce interlocking features, including molding, welding, machining, and additive manufacturing (AM). This study focuses on interlocking features produced by AM. One of the most significant advantages of AM technologies is the one-step manufacturing process of the interlocking features integrated into the part design, which reduces both costs and time while simplifying the assembly phase.

Several AM techniques and material combinations have been reported in the literature for the production of mechanical interlocking structures. Dairabayeva *et al.* [5], for instance, employed the material extrusion with thermal reaction bonding (MEX-TRB) process to manufacture such structures, successfully joining polylactic acid (PLA) with thermoplastic polyurethane (TPU) to produce components with both rigid and flexible parts. Graham *et al.* [6] investigated the directed energy deposition (DED) process for creating joints between AISI 316L and glass fiber reinforced polymer, achieving the benefits of bonded and bolted systems without an increase in weight. Oliveira *et al.* [2] described the production of mechanical interlocking structures utilizing AlSi10Mg through the powder bed fusion with laser as energy source (PBF-LB) technique, which were subsequently bonded to a polycarbonate (PC) substrate using the AddJoining technique.

The implementation of the PBF-LB technique has been demonstrated to provide several benefits, as reported by Chueh *et al.* [7]. Two interlocking mechanisms were identified: a micro-scale mechanism, leveraging the inherent surface topography of the PBF-LB process, and a macro-scale mechanism, relying on printed protrusions for physical anchoring materials. The specific surface characteristic of the PBF-LB process could be deployed and controlled, by applying different laser scanning parameters and strategies, to enhance joint adhesion strength. Proper adhesion between materials is crucial in bonding performance. Numerous studies have focused on enhancing interfacial bonding, indicating that both the shape and the strength of interlocking structures mainly influence joint retention [8]. Nguyen *et al.* [9], for instance, investigated the performance of mechanical interlocking structures, referred to as pins, produced by the PBF-LB technique. They manufactured cylindrical Ti6Al4V pins with a 45° chamfered tip, varying the pin length (L) and diameter (D) to characterize the interface strength with a carbon fiber reinforced polymer and to identify the critical L/D aspect ratio for pin performance. Additionally [10], they proposed different pin geometries, including grooved, pyramidal, and helical shapes, to assess their influence on the mechanical response of the joint. Hence, AM emerges as a crucial tool for achieving complex and optimized mechanical interlocking structures, thereby enhancing joint functionality.

This study focused on interlocking design, given its role in joint performance. An extensive literature review allowed identifying the most promising interlocking features in four distinct geometries, which were subsequently proposed in this work. The aim was to conduct a comparative analysis of the geometries and evaluate the effectiveness of PBF-LB in producing efficient AlSi10Mg interlocking structures. Some representative samples of these structures were then subjected to standard heat treatment for stress relief in order to evaluate the effect of the post treatment. The investigation analyzed and compared the resulting geometry, microstructure, and density utilizing metallographic and tomographic methods. All samples exhibited full density and good geometrical accuracy. Findings contribute to an increased understanding of designing and manufacturing efficient mechanical interlocking structures through the PBF-LB process.

2. Materials and methods

The following sections present the material and the methodology adopted for the design of the interlocking geometries, with a detailed description of the proposed features. Subsequently, the techniques used for sample production, tomographic analysis, and metallographic characterization are delineated.

2.1. Selection of the geometries

The mechanical interlocking mechanism relies on two fundamental principles: material adhesion and geometric interference. In order to achieve geometric interference, the shape of the structure must be designed in such a way as to create undercuts, which subsequently lock materials in one or multiple directions. Consequently, detailed design considerations are essential to improve the effectiveness of the joint. To this end, a literature review was conducted to identify potential interlocking geometries.

Among the analyzed geometries, the cylindrical shape emerged as the simplest and most frequently proposed. For instance, Graham *et al.* [11] demonstrated the efficacy of cylindrical features in joining AISI 316L and composite materials with an epoxy resin matrix. The results of quasi-static tests demonstrated that the joint strength increased by a range from 70% to 100% compared to joints without interlocking features. Sarantinos *et al.* [12] utilized a numerical optimization tool to refine the shape of titanium interlocking structures, suggesting the incorporation of conical tips and undercut geometries. Furthermore, intricate geometries inspired by nature were also developed, such as the structures mimicking the elytra of the diabolical ironclad beetle proposed by Li *et al.* [13]. These features demonstrated improvements in both strength and ductility at the interface between AISI 316L and Inconel 625.

The literature review revealed a wide range of geometries with a notable lack of standardization concerning geometric parameters. Nevertheless, certain features, such as undercuts, conical tip shape, chamfers or fillets [14], have been consistently emphasized across multiple studies for their significant influence on joint performance.

In accordance with the previously outlined findings, this paper proposes four interlocking geometry designs, which incorporate the features that have proven to be the most relevant. It is of note that for each of the aforementioned designs, the corresponding inspiring study is presented, which details the modifications made to the design in terms of shape and dimensions. The objective of this was to enhance the interlocking mechanism.

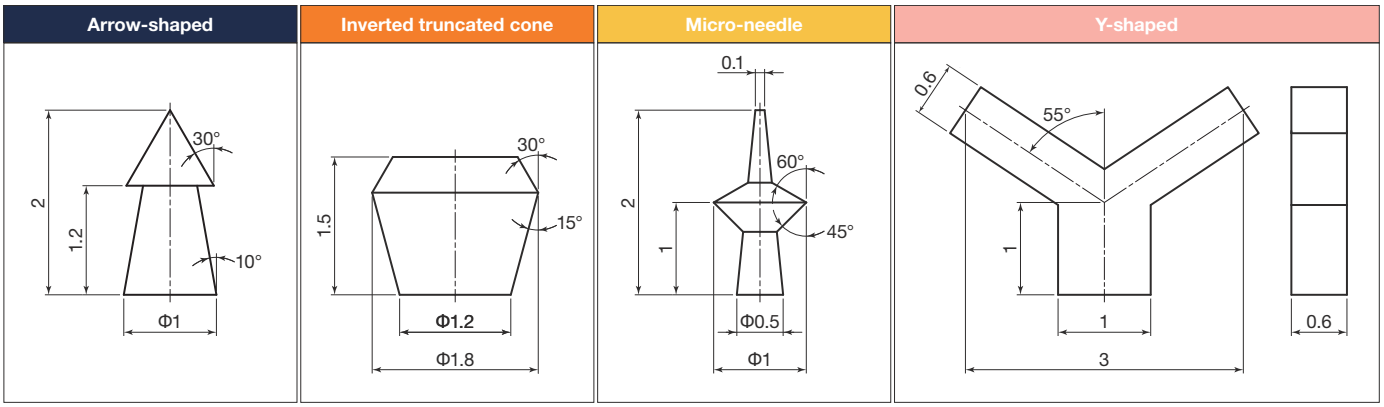

Fig. 1. Geometries of the pins.

The four proposed geometries, hereafter referred to as *pins*, are shown in Fig. 1. All the pins have dimensions in the millimeter range.

- The *arrow-shaped pin* consists of a truncated-cone body with a conical tip designed to facilitate embedding in the material to be joined. Previous studies, such as those by Parkes *et al.* [3], have explored similar shapes in the context of hybrid penetrative reinforcement (HYPER). This approach involved small arrow-shaped pins protruding from metallic parts to realize metal-composites assemblies with superior strength and toughness.
- The *inverted truncated cone pin* is derived from the structures introduced by Chueh *et al.* [7]. The top chamfer is added to enhance the material engagement and strength of the interlocking feature.
- The *micro-needle pin* draws inspiration from the effective adhesion mechanism of mosquito proboscises within the prey epidermis [15]. Amer and Chen [15] proposed a similar geometry, emphasizing the potential benefits of incorporating barbed features as mechanical interlocks, despite the increased manufacturing complexity.
- The *Y-shaped pin* is inspired by the interlocking design proposed by Alsheghri *et al.* [16], which resembles the interlocking patterns observed in the mangrove tree roots. This design utilizes the lateral sections of the Y-shape to generate undercut geometries, thereby enhancing the interlocking effect.

2.2. Fabrication

A commercially available AlSi10Mg spherical powder, with particle sizes ranging from 25 µm to 65 µm, supplied by EOS GmbH (Krailing, Germany), was used. Samples were created by arranging arrays of pins on the top surface of 10 × 10 × 5 mm³ plates, with a spacing of 1 mm between each pin. Four replicas were produced for each pin geometry, giving a total of 16 samples designated for metallographic characterization. In addition, samples consisting of a Ø6 × 10 mm³ cylindrical base with a single pin on the top were produced for tomographic analysis.

Table 1. PBF-LB process parameters employed.

Parameters	Value
Laser power	195 W
Laser spot size	100 µm
Layer thickness	30 µm
Scanning speed	800 mm/s
Hatching distance	0.17 mm

All the samples were manufactured in a single job using an EOS M270 Dual Mode machine by EOS GmbH. This PBF-LB system is equipped with a 200 W Yb-fiber laser and features a spot diameter of 100 µm at the focal plane. A controlled oxygen level below 0.1% was maintained within the building chamber by a continuous flow of argon during the process. The platform temperature was kept at 100 °C. Process parameters for AlSi10Mg were selected based on the study of Krishnan *et al.* [17] to ensure complete densification (Table 1). The scanning strategy involved the use of stripes with a width of 5 mm and a rotation of the scanning vector by an angle of 67° between consecutive layers. A soft recoater with carbon fiber brushes was used during production to avoid the risk of pin breakage.

After the production, half of the samples were removed from the building platform using the Wire-Electrical Discharge Machining (wire-EDM) e-cut system by Suzhou Baoma (Suzhou, China) to analyze them in the as-built condition. The platform with the other half of the samples was subjected to a stress-relieving heat treatment at 310 °C for 1 hour, then the samples were separated from the platform using the same wire-EDM equipment. This allowed the samples to be analyzed and compared in two conditions, as-built and heat-treated, in order to observe the influence of post treatment, if any.

2.3. Tomographic analysis and metallographic characterization

The samples underwent tomographic analysis and metallographic characterization, evaluating their geometrical accuracy, microstructure, and porosity. At first, the samples were analyzed using a Leica EZ4 W stereomicroscope by Leica Microsystems (Wetzlar, Germany) to verify the morphology of the pin arrangements. Computed tomography (CT) was then conducted using Phoenix V|tome|x S240 by Baker Hughes (Houston, TX, USA). The CT scans were performed using a voltage of 100 kV and a current of 85 µA, resulting in a voxel size of approximately 8 µm. The data obtained from the scans were then processed using Phoenix datos|x 2 reconstruction

software. The software VGSTUDIO MAX 3.5 by Volume Graphics (Heidelberg, Germany) was used to compare nominal and actual geometries and to perform porosity analysis.

For the metallographic characterization, the samples were mounted with a non-conductive transparent resin and ground along the building direction using SiC grinding papers (800, 2500, and 4000 grit size). Subsequently, they were polished to a 3 µm finish using diamond suspension, followed by alumina suspensions (0.2 µm). Etching with Keller solution for 10 seconds was then employed to reveal microstructural features, such as grains and melt pool boundaries. The microstructural examination was performed using both a light optical microscope (LOM) Leica DMI 5000 M by Leica Microsystems and a scanning electron microscope (SEM) Phenom XL by Phenom-World BV (Eindhoven, The Netherlands).

3. Results and discussion

The subsequent sections delineate the dimensional accuracy of geometries, demonstrating the effectiveness of the PBF-LB in producing mechanical interlocking structures. Subsequently, the microstructure of the sample is examined, highlighting the effects of the post treatment. Finally, the density characteristics exhibited by the specimens are discussed.

3.1. Dimensional accuracy analysis

Process performance was assessed by an initial observation of the pins using the stereomicroscope. Two images for each sample were captured to observe both the top and the side of the pins (Fig. 2). This preliminary analysis confirmed successful pin manufacturing, exhibiting the characteristic rough surface typical of the PBF-LB process, alongside identifiable defects such as balling. Furthermore, no significant differences were noted between the as-built and heat-treated samples, which is in line with the expected outcomes. Hence, this section presents the findings from the analysis performed on the as-built pins, which are valid for both conditions.

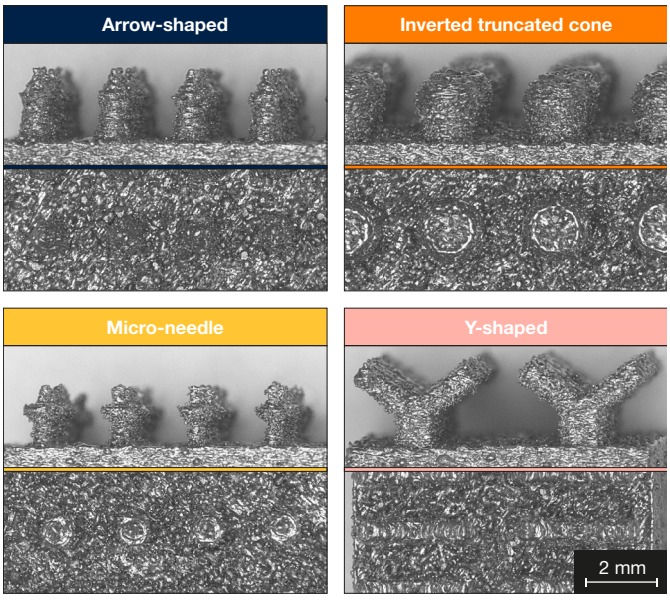

Fig. 2. Top and side views of the produced pins.

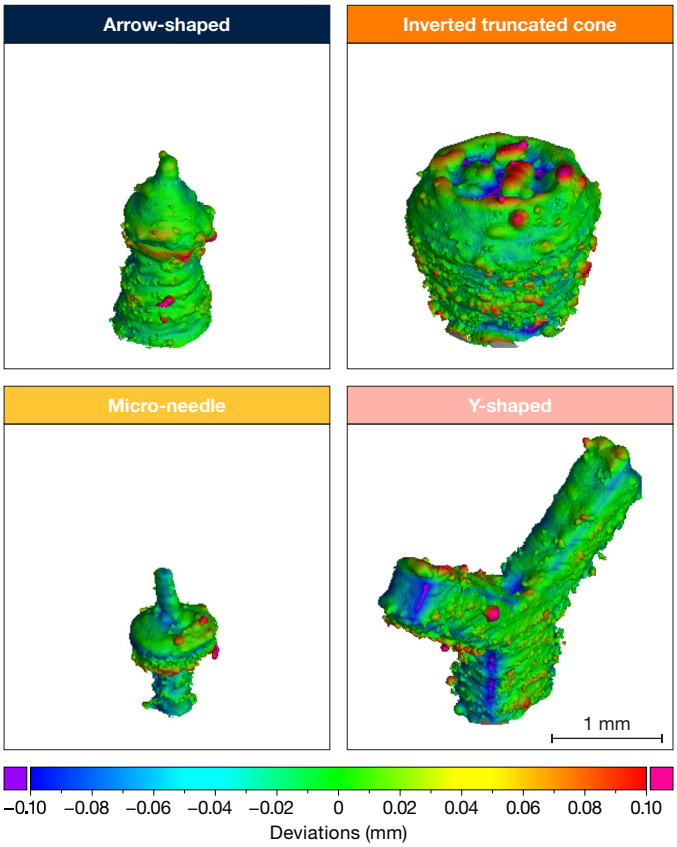

Fig. 3. Deviation maps of the actual geometries vs the nominal ones.

To assess the dimensional accuracy of the samples, a nominal/actual analysis was conducted using VGSTUDIO MAX 3.5 software. The actual geometry of the samples, reconstructed from the CT scans, was compared with the nominal geometry to evaluate dimensional deviations. The alignment between the geometries was achieved using a feature-based registration algorithm, which identifies the significant features of the object for fitting and minimizing the errors. Fig. 3 illustrates the colored deviation maps, showing the differences between the actual and nominal geometries.

The analysis revealed that 95% of the actual surfaces had a maximum absolute deviation of approximately 0.10 mm from the nominal surfaces, equal to the laser spot. Specifically, all four geometries exhibited an overall good alignment with the nominal surfaces, presenting slight negative deviations below 0.10 mm distributed across the pins. This consistent pattern could be attributed to the shrinking phenomena associated with the cooling phases inherent to the PBF-LB process. However, limited exceptions from the overall trend emerged, mainly due to geometric errors or balling issues.

Geometric errors became evident when the required geometry involved features with relatively small dimensions. This was observed, for example, in the micro-needle shaped pin, in which the whole tip, whose diameter matches the laser resolution, showed negative deviations ranging from 0.08 mm to 0.10 mm (in blue in Fig. 3). Similarly, the challenges in manufacturing certain features, such as curved or inclined surfaces, inherent to the PBF-LB process, could lead to negative deviations, as observed in the lateral surfaces of the Y-shaped pin (in blue in Fig. 3). Conversely, isolated macro

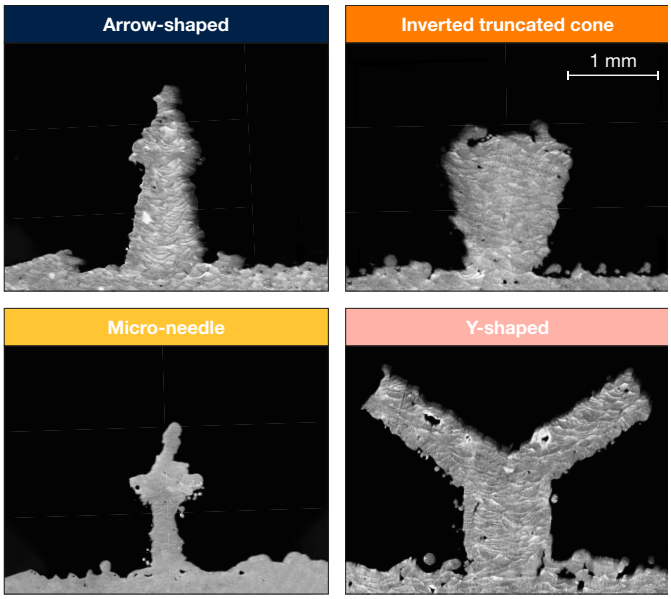

Fig. 4. Microstructures acquired by the optical microscope after etching. Melt pools are clearly visible in the OM images.

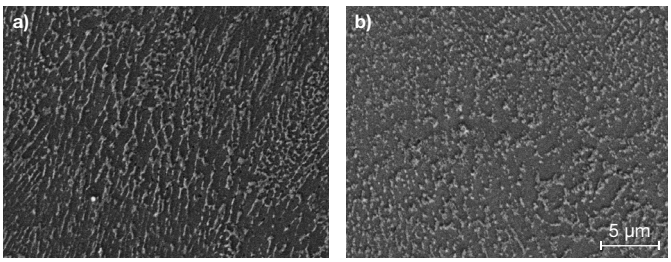

Fig. 5. SEM images showing the cellular structure of the (a) as built and (b) heat-treated arrow shaped pin.

defects exceeding the nominal surfaces by a range between 0.08 mm and 0.10 mm were found on larger areas, such as the top surface of the inverted truncated cone shaped pin (in red/purple in Fig. 3). These defects could be attributed to balling phenomena, as confirmed by the previous stereomicroscope analysis. It can be concluded that the expected features were achieved for all pins, closely adhering to design requirements, highlighting the effectiveness of PBF-LB in producing such structures.

3.2. Microstructure analysis

The microstructure of the polished and etched samples was examined using optical microscopy. For each pin geometry, images of the cross-section parallel to the build direction were acquired at a 5x magnification. It is well known that as the laser beam melts the powder material during the process, it generates a liquid pool named the melt pool. The scanning strategy adopted in this study produced semi-circular shaped melt pools, all uniformly oriented and partially overlapped on the previous tracks, as shown in Fig. 4.

The cross section along the build direction was also examined using the scanning electron microscope at higher magnification, focusing on melt pool boundaries. This revealed a fine cellular-dendritic structure attributed to the high solidification rate. The comparison between the as-built and heat-treated samples revealed a notable difference. The as-built samples showed elongated cells of primary α-Al surrounded by a continuous Si network (Fig. 5a). After the heat treatment, an enlargement of the cells was evident (Fig. 5b). The silicon network surrounding the primary α-Al cells broke down, creating isolated and distinguishable Si particles. This phenomenon is known to enhance ductility but also leads to a reduction in yield stress, as reported in the literature [18].

3.3. Porosity analysis

Porosity analysis was performed using VGSTUDIO MAX 3.5 software. The VGEasyPore algorithm was applied to identify pores within a defined region based on the gray value of the voxels compared to a specified contrast threshold. Therefore, voxels are marked as defects if their gray value differs from the gray value of the voxels associated with the component material by a quantity larger than the threshold. Defects were calculated with subvoxel accuracy.

Fig. 6 illustrates the distribution of porosities and their diameters in the three-dimensional reconstructions of the pins. It is important to notice that, as expected, no significant differences were noted between the as-built and heat-treated samples. For this reason, the findings relating to the heat-treated samples are presented herein, however the observations are equally valid for both conditions. The samples exhibited uniformly distributed porosity with an average diameter lower than 0.20 mm (shown in blue in Fig. 6). The presence of small pores, particularly near the base of the pins, could be attributed to gas entrapment, possibly due to rapid cooling rates induced

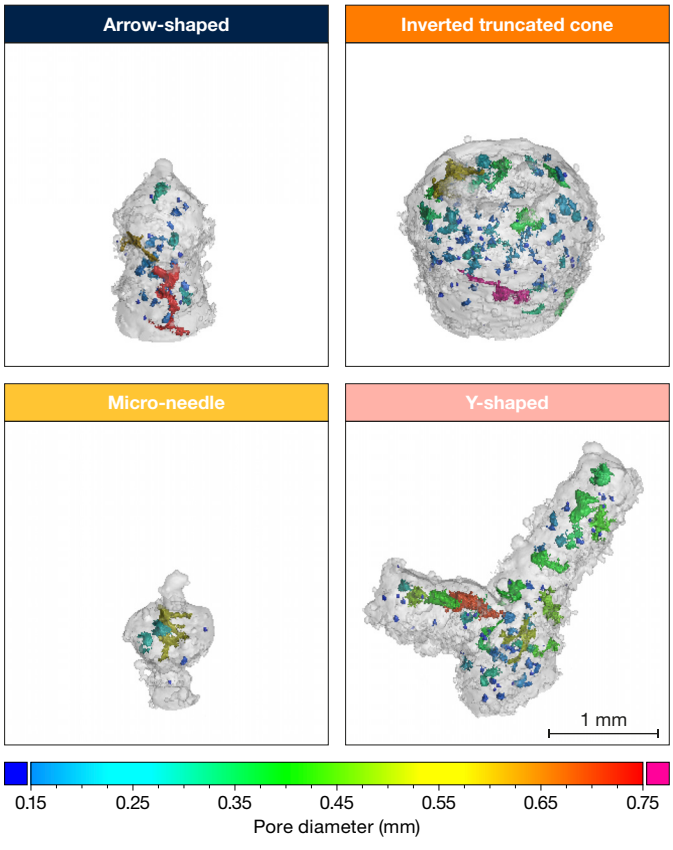

Fig. 6. Porosity distribution analysis of the heat-treated pins.

by substrate heat dissipation. Porosities with an average diameter ranging from 0.32 mm to 0.50 mm (in green in the Fig. 6) were observed on the top surface of the inverted truncated cone shaped pin and in the lateral sections of the Y-shaped pin. These observations are consistent with the issues identified in the previous section through the nominal/actual analysis. Additionally, a few larger porosities with an average diameter above approximately 0.65 mm (in red/purple in Fig. 6) were observed in the central and lateral regions of the pins. These defects may be indicative of a lack of fusion due to their elongated shape.

In terms of defect volume ratio (DVR), the Y-shaped pin has the highest ratio, approximately around 2.8%. The arrow-shaped pin is the second most porous, with a DVR percentage of about 1.4%. The inverted truncated cone has a DVR of 1.0%, followed by the micro-needle shaped pin, which has the lowest presence of pores, with a DVR of 0.8%. Overall, the presence of defects is acceptable, indicating a positive outcome of the manufacturing process. It is noteworthy that the software algorithm relies on grey level gradients to detect porosities, and this process can be negatively influenced by artifacts generated during CT scanning. As a result, the general trend of porosity is evident, but quantification may be affected by errors.

4. Conclusions

This research investigated the potential of the PBF-LB process in producing efficient mechanical interlocking structures for joining dissimilar materials, addressing the growing demand for lightweight and functional components. Considering the crucial role of interface design in joint effectiveness, significant attention was directed to the design of mechanical interlocking structures. Four geometries, including an arrow-shaped, an inverted truncated cone, a micro-needle, and a Y-shaped pin, were proposed. Three main findings emerged from the study.

- The dimensional accuracy analysis of the structures revealed that 95% of the surfaces closely matched the nominal surfaces, with maximum absolute deviations of approximately 0.1 mm, primarily attributed to inherent process phenomena. Despite isolated macro defects, all pins achieved the expected features, maintaining overall alignment with the design specifications.
- The post-processing heat treatment applied to the AlSi10Mg samples resulted in significant microstructural changes, characterized by the enlargement of primary α-Al cells and breakdown of the surrounding Si network, consistent with literature findings. No differences were observed in terms of geometry and density.
- The porosity analysis indicated the existence of uniformly distributed small pores in the central region of all pins, in addition to isolated larger porosity. The DVR was found to range between 0.8% and 2.8%. This evidence suggests that the presence of defects in the pins may be limited, although the quantification may be influenced by artifacts associated with the CT scanning process.

The detailed analysis of the interlocking structures demonstrated the feasibility of achieving dense and accurate pins through the PBF-LB process, paving the way for enhanced functionality and sustainability in various industrial applications. The examined structures appear to be a promising alternative to conventional joining methods. However, further investigations are essential to explore the joining with other materials and the overall behavior of the multi-material joint.

Acknowledgements

The authors acknowledge the Italian MUR for its funding of the project PRIN 2020 “TARGET – addiTive mAnufactuRing for liGhtwEight joinTs”, Grant Number CUP E15F22000640001TARGET.

References

[1] Ouyang Y, Chen C. Research advances in the mechanical joining process for fiber reinforced plastic composites. Compos Struct 2022; 296:115906.
[2] Oliveira GHM, Belei C, de Carvalho WS, Canto LB, Amancio-Filho ST. On the fully additive manufacturing of PC/AlSi10Mg hybrid structures. Mater Lett 2023; 330:133378.
[3] Parkes PN, Butler R, Meyer J, de Oliveira A. Static strength of metal-composite joints with penetrative reinforcement. Compos Struct 2014; 118:250-6.
[4] Mustafa I, Kwok T-H. Development of Intertwined Infills to Improve Multi-Material Interfacial Bond Strength. J Manuf Sci Eng 2021; 144:
[5] Dairabayeva D, Perveen A, Talamona D. Investigation on the mechanical performance of mono-material vs multi-material interface geometries using fused filament fabrication. Rapid Prototyping J 2023; 29:40-52.
[6] Graham DP, Rezai A, Baker D, Smith PA, Watts JF. The development and scalability of a high strength, damage tolerant, hybrid joining scheme for composite–metal structures. Composites Part A 2014; 64:11-24.
[7] Chueh Y-H, Wei C, Zhang X, Li L. Integrated laser-based powder bed fusion and fused filament fabrication for three-dimensional printing of hybrid metal/polymer objects. Addit Manuf 2020; 31:100928.
[8] Sarantinos N, Tsantzalis S, Ucsnik S, Kostopoulos V. Review of through-the-thickness reinforced composites in joints. Compos Struct 2019; 229:111404.
[9] Nguyen ATT, Brandt M, Feih S, Orifici AC. Pin pull-out behaviour for hybrid metal-composite joints with integrated reinforcements. Compos Struct 2016; 155:160-72.
[10] Nguyen ATT, Amarasinghe CK, Brandt M, Feih S, Orifici AC. Loading, support and geometry effects for pin-reinforced hybrid metal-composite joints. Composites Part A 2017; 98:192-206.
[11] Graham DP, Rezai A, Baker D, Smith PA, Watts J. A hybrid joining scheme for high strength multimaterial joints. 18th International Conferences on Composite Materials 2011;
[12] Sarantinos N, Kostopoulos V, Di Vita G, Campoli G, Bricout L. Micro-pins: the next step in composite–composite and metal–composite joining. CEAS Space J 2019; 11:351-8.
[13] Li X, Jiang P, Nie M, Liu Z, Liu M, Qiu Y, Chen Z, Zhang Z. Enhanced strength-ductility synergy of laser additive manufactured stainless steel/Ni-based superalloy dissimilar materials characterized by bionic mechanical interlocking structures. J Mater Res Technol 2023; 26:4770-83.
[14] Nguyen ATT, Pichitdej N, Brandt M, Feih S, Orifici AC. Failure modelling and characterisation for pin-reinforced metal-composite joints. Compos Struct 2018; 188:185-96.
[15] Amer M, Chen RK. Self-Adhesive Microneedles with Interlocking Features for Sustained Ocular Drug Delivery. Macromol Biosci 2020; 20:2000089.
[16] Alsheghri AA, Alageel O, Amine Mezour M, Sun B, Yue S, Tamimi F, Song J. Bio-inspired and optimized interlocking features for strengthening metal/polymer interfaces in additively manufactured prostheses. Acta Biomater 2018; 80:425-34.
[17] Krishnan M, Atzeni E, Canali R, Calignano F, Manfredi D, Ambrosio EP, Iuliano L. On the effect of process parameters on properties of AlSi10Mg parts produced by DMLS. Rapid Prototyping J 2014; 20:449-58.
[18] Trevisan F, Calignano F, Lorusso M, Pakkanen J, Aversa A, Ambrosio EP, Lombardi M, Fino P, Manfredi D. On the Selective Laser Melting (SLM) of the AlSi10Mg Alloy: Process, Microstructure, and Mechanical Properties. Materials 2017; 10:76.